A New Look into the Impacts of the Dust Radiative Effects on the Energetics of Tropical Easterly Waves

Farnaz E Hosseinpour[1,2] and Eric M Wilcox[1]

[1] Desert Research Institute

Reno, NV, USA

[2] University of Nevada, Reno

Reno, NV, USA

Corresponding author's email address: Farnaz@dri.edu

Keywords

Saharan Air Layer, dust, aerosol radiative effect, wave activity, eddy kinetic energy, tropical Atlantic Ocean, African easterly jet, African easterly waves, MERRA-2, MODIS

Abstract

Saharan dust aerosols are often embedded in tropical easterly waves, also known as African easterly waves, and are transported thousands of kilometers across the tropical

Atlantic Oceans, reaching the Caribbean Sea, Amazon Basin, and the eastern U.S. However, due to the complex climate dynamics of West Africa and the eastern tropical Atlantic Ocean, there is still a lack of understanding of how dust particles may influence the development of African easterly waves, which are coupled to deep convective systems over the tropical Atlantic Ocean and in some cases may seed the growth of tropical cyclones. Here we used 22 years of daily satellite observations and reanalysis data to explore the relationships between dust in the Saharan air layer and the development of African easterly waves. Our findings show that dust aerosols are not merely transported by the African easterly jet and the African easterly waves system across the tropical Atlantic Ocean, but also contribute to the changes in the eddy energetics of the African easterly waves.

The efficiency of dust radiative effect in the atmosphere is estimated to be a warming of approximately 20 Wm^{-2} over the ocean and 35 Wm^{-2} over land. This diabatic heating of dust aerosols in the Saharan Air Layer acts as an additional energy source to increase the growth of the waves. The enhanced diabatic heating of dust leads to the increase in meridional temperature gradients in the baroclinic zone, where eddies extract available potential energy from the mean-flow and convert it to eddy kinetic energy. This suggests that diabatic heating of dust aerosols can increase the eddy kinetic energy of the African easterly waves and enhance the baroclinicity of the region. Our findings also show that dust outbreaks over the tropical Atlantic Ocean precede the development of baroclinic waves downstream of the African easterly jet, which suggests that the dust radiative effect has the capability to trigger the generation of the zonal and meridional transient eddies in the system comprising the African Easterly Jet and African easterly waves.

1   Introduction

African Easterly Waves (AEWs), also known as tropical Atlantic easterly waves, are synoptic-scale atmospheric disturbances with a preferred wavelength in the 2000-4000km range that often develop into tropical Atlantic cyclones (Dunn, 1940). The basic characteristics and behavior of the AEWs have been described in previous studies (Charney and Stern, 1962; Chang, 1993; Kiladis et al., 2006; Diaz and Aiyyer, 2013). Local heating is a dominant factor in determining the growth of AEWs over West Africa (Norquist et al., 1977), such that the presence of diabatic heating near the entrance of the African Easterly Jet (AEJ) is a favorable factor in generating AEWs (Thorncroft et al., 2008; Russell et al., 2020). The localized mid- to lower-tropospheric heating generates vortices in the vicinity of the AEJ core, which is the genesis of the AEWs (Thorncroft et al., 2008; Berry and Thorncroft, 2012). AEWs can be initiated by convective triggers over the highlands of eastern Africa and forcing from the subtropical Atlantic storm track (Cornforth et al. 2009).

Several studies have shown that AEWs are intensified in the presence of convective systems where the mesoscale convection and synoptic-scale AEWs are dynamically coupled (Kiladis et al., 2006; Hsieh and Cook, 2005&2007; Berry and Thorncroft, 2012). A large portion of tropical Atlantic cyclones and hurricanes evolve from the AEWs (Avila and Clark, 1989; Avila and Pasch, 1992; Pasch and Avila, 1994) during the boreal summer seasons, which is the season when the amplitude of AEWs peaks (e.g., Roundy and Frank, 2004).

Numerous studies addressed the dynamics of the AEWs; however, the impacts of aerosol radiative effects on the energy of the AEWs are poorly understood. The Sahara Desert in North Africa is the largest source of dust in the world, where over sixty million

tons of dust particles (e.g., Prospero and Lamb, 2003; Lau and Kim, 2007) are lifted annually and transported within the Saharan Air Layer (SAL) across the Atlantic Ocean (Carlson and Prospero, 1972) and reaches the Caribbean Sea, the Gulf of Mexico, Amazon Basin and the United States (e.g., Perry et al., 1997; Liu et al., 2008, Francis et al., 2020). Dust particles in the SAL have a robust influence on regional and global climate through their impacts on radiation, clouds, hydrological cycle, and atmospheric circulation (Colarco et al., 2003; Lau et al., 2009; Wilcox et al., 2010; Kim et al., 2010). In particular, among aerosol species, dust is known for having a strong shortwave radiative effect by both efficiently scattering, as well as absorbing, incoming radiation and leading to a heating of the dust layer and strong cooling of the surface (Myhre et al., 2004; Mamun et al., 2021, Francis et al., 2022). The shortwave radiative effect is slightly counteracted by the longwave radiative effect of dust which causes warming at the surface and cooling within the atmosphere (Meloni et al., 2018).

A limited number of studies have focused on the impacts of Saharan dust plumes on the dynamics of the AEWs (Jones et al., 2003; Ma et al., 2012; Hosseinpour and Wilcox, 2014). Jones et al. (2004) suggested that dust optical and radiative properties have significant impacts on the AEWs. They showed that the low-level temperature anomalies associated with the AEWs are modulated by the dust radiative effect and suggested that dust loading in the SAL precedes the maximum geopotential height at 700-hPa by about 1-2 days. Model sensitivity studies have also shown that the intensification of AEWs can be induced by dust (Ma et al., 2012; Grogan et al., 2019; Bercos-Hickey and Patricola, 2021; Grogan et al., 2022). The analytical and numerical study of Grogan et al. (2016) found that the presence of dust enhances the development of AEWs by providing a

1   buoyancy source. They also showed that dust can affect the propagation of AEWs by

2   changing the wind shear and stability of the atmosphere. Using a regional climate model

3   coupled with a dust model, Bercos-Hickey et al. (2017) found that Saharan dust causes

4   AEJ to shift northward, upward, and westward, and this results in westward expansion and

5   the northward shift of both the northern and southern tracks of the AEWs. Satellite

6   observations support this notion by showing that a similarity exists between the pattern of

7   temperature and wind anomalies of the AEWs and those associated with the dust outbreaks

8   (Hosseinpour and Wilcox, 2014).

9   Saharan dust is not the only contributor to aerosol radiative effect over Africa and

10   the Atlantic Ocean. Previous studies showed that smoke transport from biomass burning

11   can reach up to ~ 3-5 km altitude, which is above the stratocumulus clouds over the Sahel

12   region, and may affect the radiation through aerosol direct and indirect effects (Redemann

13   et al., 2021). Biomass burning in Africa is closely related to seasonal rainfall variability

14   and the location of the Intertropical Convergence Zone (ITCZ); thus, the emissions from

15   biomass burning in North Africa occur in boreal spring and winter, when ITCZ is south

16   of the equator (e.g., Cahoon et al., 1992; Barbosa et al., 1999; Ramo et al., 2020). During

17   the boreal winter, smoke aerosols are maximized over the Sahel region (Figure 1,

18   Haywood et al., 2008), where the northward transport of smoke merges with dry

19   southward and westward transport of dust aerosols. This leads to the co-existence of dust

20   and smoke, as smoke is dominated on the top of the dust layer (Haywood et al., 2008).

21   However, during the boreal summer, biomass burning mainly occurs in South Africa,

22   where the air circulations transport smoke plumes toward the South-East Atlantic off-

23   coasts of Namibia and Angola (Zuidema et al., 2016; Cochrane et al., 2022). To study the

1 effects of Saharan dust aerosols on AEWs with avoiding the major impact of smoke

2 transport from biomass burning in South Africa, we focus our study on the region above

3 $5°$ N latitude in West Africa and the eastern Atlantic Ocean in boreal Summer, where the

4 contribution of aerosols from biomass burning is less than 15% by mass over this region

5 (Matsuki et al., 2010). This study focuses on boreal summer season, because during this

6 season, the amplitude of AEWs peaks (e.g., Roundy and Frank, 2004), and Saharan dust

7 storms are active with less simultaneous transport of smoke from South Africa biomass

8 burning.

9   While previous studies showed the impacts of dust aerosols on climate (Ming and

10 Ramaswamy, 2011; Hosseinpour and Wilcox, 2014; Chen et al., 2021; Liang et al., 2021;

11 Grogan et al., 2022), hydrological cycle (Konare et al., 2005; Kim et al., 2010; Bercos-

12 Hickey et al., 2020) and cloud properties (Weinzierl et al., 2017; Haarig et al., 2019),

13 these elements of the climate system in this region exhibit strong variability due to AEWs.

14 To understand the details of interactions between dust aerosols and climate over the

15 Atlantic Ocean, it is essential to understand how the evolution of AEWs is determined by

16 both diabatic heating, as well as exchanges of eddy kinetic energy (EKE) within the jet-

17 wave system and how dust may contribute to the energy driving AEWs. Toward this goal,

18 we apply eddy energetic concepts to further analyze the relationships between dust and

19 the AEJ-AEWs system to gain insight into the impacts of the dust aerosol radiative effects

20 on the development of AEWs and the distribution of kinetic energy from the source of

21 instability (i.e., AEJ). Section 2 summarizes the data and methodology. Section 3

22 discusses the summary of results: the climatology and variability of the AEJ-AEWs

23 system from an energy point of view (3.1), climatology and variability of Saharan dust

1   aerosols across West Africa and the eastern tropical Atlantic Ocean (3.2), and the impacts

2   of dust on the AEJ-AEWs system (3.3). Conclusions are presented in Section 4.

4   **2   Data and methodology**

5   This study focuses on the relationships of Saharan dust aerosols and AEWs in

6   boreal summer, because during this season, the amplitude of the AEW peaks (e.g., Roundy

7   and Frank, 2004). We used a 22-year time series of NASA's satellite observations and

8   reanalysis for the boreal summer seasons from June to August (JJA) 2000-2021 to calculate

9   the variability of energy components of the system comprising the AEJ, the AEWs, and

10   the aerosol radiative effect.

12   **2.1   MODIS and MERRA-2 data**

13   To study the climatology of West Africa and the eastern tropical Atlantic Ocean,

14   the successor to the Modern Era Retrospective-analysis reanalysis (MERRA; Rienecker et

15   al., 2008; 2011), the 3-hourly MERRA-2 (Randles et al., 1980, 2017; Buchard et al., 1980;

16   Gelaro et al., 2017) were used to provide more reliable assessments of climatic and

17   meteorological variables from 1980 to the present. The MERRA-2 reanalysis has a 3-

18   hourly temporal resolution and a spatial resolution of 0.5° latitude by 0.625° longitude with

19   72 vertical levels, extending from the surface up to 0.01-hPa.

20   We used the MERRA-2 atmospheric radiative effect that is broad band shortwave

21   flux across the visible spectrum to study aerosol radiative effect as described in Section

22   2.2, as well as the meteorological variables, including wind components, temperature,

23   pressure and humidity from the 3-hourly MERRA-2 reanalysis for the boreal summer (JJA)

1   from 2000 to 2021, to calculate the eddy energetic terms of the AEW-AEJ system as

2   described in Section 2.3.

3   The reason for choosing the MERRA-2 analysis for this study is as follows: An

4   essential aspect of MERRA-2 is the assimilation of bias-corrected aerosol optical depth

5   (AOD) from the various ground- and space-based remote sensing platforms (e.g., Randles

6   et al., 2017). In particular, AOD is simulated in MERRA-2 with a radiatively coupled

7   version of the Goddard Chemistry, Aerosol, Radiation, and Transport (GOCART; Colarco

8   et al., 2010) aerosol model. In this manner, the MERRA-2 system provides an estimate of

9   the atmosphere state historically from the present day back to 1980. It is important to note

10 that the dust and the circulation are fully coupled in MERRA-2. Using such an empirical

11 tool, it is not possible to directly compare a complete representation of the circulation

12 without dust to the circulation with dust. However, the benefit of using MERRA-2 is that

13 it offers a more realistic representation of the circulation than an unconstrained model

14 because of the data assimilation. It is our intention with this study to evaluate the empirical

15 relationships between the dust radiative effect and the energetics of AEWs in a reanalysis

16 constrained by observations, which can be compared with the results of a follow-on

17 examination of a controlled experiment in an unconstrained atmospheric general

18 circulation model comparing simulations with dust radiative effects to simulations without

19 dust radiative effects.

20   To evaluate the MERRA-2 reanalysis with satellite observations, we used the

21   entire record of the daily AOD (level 3) from two independent algorithms and well-

22   calibrated sensors: (I) the 550-nm Moderate Resolution Imaging Spectro-radiometer dark-

23   target retrieval (MODIS, MOD08_D3; Remer et al., 2021 with a 1° spatial resolution on

1   Terra since 2000 for the dust domains over the Atlantic Ocean, and (II) the 470-nm Deep

2   Blue (Sayer et al., 2019; Hsu et al., 2019) retrievals of MODIS AOD available with a 1°

3   spatial resolutions for the dust source regions over the land in boreal summer (JJA, 2000-

4   2021). The summary of the information about MODIS and MERRA-2 data product name,

5   variables, spatial and temporal resolutions are provided in Table 1.

7   **2.2   Aerosol radiative effect in the atmosphere**

8   We used the components of aerosol radiative effect at the surface and top of the

9   atmosphere (TOA) from the 3-hourly MERRA-2 reanalysis datasets to calculate the

10   radiative effect of dust in the atmosphere (i.e., TOA minus surface) as follows:

11    $$F_{aerosol} = \left(SWF_{TOA_{tot}} - SWF_{TOA_{clean}}\right) - \left(SWF_{sfc_{tot}} - SWF_{sfc_{clean}}\right) \qquad \text{Eq. (1)}$$

12   where $SWF_{TOA_{tot}}$ refers to the net downward shortwave radiation flux at the TOA,

13    $SWF_{TOA_{clean}}$ is the net downward shortwave flux at TOA under clean-sky condition,

14    $SWF_{sfc_{tot}}$ is the net downward shortwave flux at the surface, and $SWF_{sfc_{clean}}$ is net

15   downward shortwave flux at the surface under clean-sky condition.

16   To show the variability of dust, the time-longitude Hovmöller diagrams of daily

17   anomalies of aerosol radiative effect are provided to represent the dust transport within

18   SAL across the tropical Atlantic Ocean. The daily values of radiative effect are calculated

19   by time averaging the 3-hourly data. The daily anomalies of radiative effect were calculated

20   with respect to the seasonal time-average of radiative effect for each year. These anomalies

21   were latitudinally averaged over the latitudes of dust domains, 12-22° N.

1   To investigate the relationship between dust and the AEJ-AEWs system over the

2   Atlantic Ocean, we focused on the dust variability over the ocean; therefore, we consider

3   the location of the SAL over the tropical Atlantic Ocean, the so-called OSAL domain,

4   where dust is significant from -28° to -16° E Longitude and from 12° to 22° N latitude in

5   the climatology of boreal summer seasons.

6   **2.3   Energetics of the AEJ-AEWs system**

7   We used MERRA-2 meteorological variables as described in Section 2.1, to

8   calculate the eddy energetic terms associated with the distribution of kinetic energy across

9   the AEJ-AEWs system for the boreal summer from 2000 to 2021. While the MERRA-2

10   data is 3 hourly, we averaged them for each day to be consistent with the daily temporal

11   resolution of MODIS AOD data. We provided daily MERRA-2 data to apply them for the

12   calculation of the eddy energetics terms.

13   From an energy point of view, the kinematics of the atmosphere is a combination

14   of mean kinetic energy (MKE) of the background mean flow and eddy kinetic energy

15   (EKE) representing transient eddies (Lorenz, 1954). The MKE associated with the AEJ is

16   calculated as below, where *u* and *v* are horizontal components of wind and bar represents

17   the time-averaged over the long-term daily time series of the wind components:

18   $$MKE = \frac{1}{2}\left(\overline{u^2} + \overline{v^2}\right)$$ Eq. (2)

19   To detect the 2-6 day and 6-11 day variations associated with the AEWs, we used

20   the methodology following Wu et al. (2013). While many studies have focused exclusively

21   on 2-6 day period AEWs, several studies have found evidence that AEWs exist on two

22   distinct time scales of 2-6 and 6-11 day periods, as the structure of the AEWs differs

1 substantially between these two different time windows (Mekonnen et al. 2006; Wu et al.,

2 2013). The time-filtering method described below was applied to decompose EKE of the

3 AEWs at different time-scale: 2-6 day and 6-11 day filtered variations.

4   We provide the daily times series of wind components by time averaging over the

5 3-hourly MERRA-2 datasets. We further used the Lanczos bandpass filtering techniques

6 described in Duchon's (1979) study to filter the 2-6 and 6-11 day disturbances from the

7 daily time series of the zonal and meridional components of wind (u, v). The daily

8 anomalies (u', v') of wind components (u, v) were calculated for each boreal summer season

9 with respect to the average of that season ($u' = u - \bar{u}$ and $v' = v - \bar{v}$; primes indicate

10 daily anomalies, and bars show seasonal averages). Finally, EKE was calculated as the

11 average of the variances of u and v shown as follows:

$$EKE = 1/2 \left(\overline{u'^2} + \overline{v'^2} \right)$$
Eq. (3)

13 The bars indicate the average over the entire JJA, 2000-2021, and the primed quantities

14 denote the deviation of wind components from the time-mean (daily anomalies) described

15 above.

16   Baroclinic conversion (BCC) is one of the most important components in the eddy

17 energy budget to distribute transient energy from the upstream baroclinic source across the

18 storm tracks downstream of the jetstream (e.g., Orlanski and Katzfey, 1991; and Chang et

19 al., 2002). The initiation of and the growth of the waves are significantly related to BCC,

20 where the transient eddies extract energy from the mean-flow through BCC (e.g., Plumb,

21 1986). Following the approach described in Chang et al. (2002) study, we calculated the

22 BCC term as below:

$$BCC = -\overline{\omega'\alpha'} \qquad \text{Eq. (4)}$$

2   where ω is the rate of pressure ($\omega = \frac{dp}{dt}$) and α is a scale to estimate the changes in the

3   vertical profile of the gradient of geopotential height ($\alpha = -\frac{\partial \emptyset}{\partial p}$). We investigate BCC to

4   identify the locations favorable for developing EKE in the AEJ-AEWs.

6   **2.4   Composite analysis**

7   The composite analyses for 2-6-day and 6-11-day variations of the eddy energetics

8   of the AEWs were conducted for the boreal summer seasons of 22 years, 2000-2021.

9   Composite EKE was calculated by subtracting the EKE values associated with the lower-

10   quartile radiative effect of dust from those EKE values associated with upper-quartile

11   aerosol radiative effect. We find the upper- and lower-quartile aerosol radiative effect

12   offshore, where the dust load is significant over the OSAL domain (rectangle in Figure 2a).

13   To determine the upper- and lower-quartile of aerosol effect, the aerosol effect over the

14   OSAL box is averaged at each time to create a time series of OSAL aerosol effect. The

15   daily time series of aerosol radiative effect of the grid points were spatially averaged over

16   the OSAL domain, which provided one single value of aerosol radiative effect for each

17   individual day in the long-term time series over the dust domain. For averaging over the

18   OSAL domain, area-weighted average is applied since the area of grid cells are not the

19   same. These time series of aerosol radiative effect were used to select the days of the upper

20   quartile and the lower quartile aerosol radiative effect for the summer season of each year.

21   Hence, we selected 23 days of the highest aerosol concentration (upper-quartile) and 23

22   days of the lowest aerosol concentration (lower-quartile) over each domain during boreal

1   summer of each year. From a climatology point of view, we used the upper quartile and

2   lower quartile of dust over 22 years of data, such that there are 506 data points to represent

3   the days with high values of dust concentration and 506 days with low values of dust over

4   each domain of study.

5   Composite EKE is provided for each grid point by subtracting the EKE values

6   corresponding to the upper-quartile dust days from those of the lower-quartile dust days.

7   Using the method explained above, the composite of the variance of zonal wind $(\overline{u'^2})$, the

8   variance of meridional wind $(\overline{v'^2})$, and the transient momentum fluxes $(\overline{u'v'})$ were also

9   calculated for boreal summer seasons, JJA, 2000-2001 (Figure 1).

10   **2.5   Time-lag analysis**

11   The time-lag analyses were conducted over each domain of study based on the

12   following processes. Using the same methodology explained above (Section 2.4.), we used

13   the time series of aerosol radiative effect spatially averaged over the dust domain to select

14   the days in the upper quartile and the lower quartile aerosol radiative effect, such that there

15   are 506 data points to represent the days with high values of dust concentration and 506

16   days with low values of dust concentration over each domain. For every 506 days of high

17   dust concentration, we studied the time series for five days before and five days after the

18   event to investigate the evolution of each individual dust storm. For each time series, we

19   assigned each day of 506 days as follows: T = 0 for the dust-peak, T = 1 for one day after

20   the dust-peak, T = -1 for one day before the peak of dust, and continue this for five days

21   before and after every 506 days. We used each of these time series for 22 years and average

22   dust radiative effect individually for T = 0, T = +/- 1, T = +/- 2, T = +/- 3, T = +/- 4, and

1   T= +/- 5 to gain insight into the climatology of dust evolution five days before and five

2   days after dust peaks over each domain. We repeated the steps explained above for the 506

3   data points of dust in the lower quartile to provide the long-term time series of low aerosol

4   radiative effect over the dust domain. Finally, by subtracting the time series of the lower

5   quartile from the upper quartile radiative effect, we provide the composite of dust over

6   each domain to investigate the highest variability of dust (as T = 0, Figure 5) and its

7   evolution five days before and after over dust domain. Using the same methodology, we

8   analyzed the wave activity that coincides with the upper quartile (and lower quartile)

9   aerosol radiative effect to investigate a possible time-lag between the dust and the

10   development of kinetic energy over the northern and southern track of the AEWs. The

11   domains selected to investigate wave activity are shown in Table 2.

13   **3   Summary of the results**

14   **3.1   AEJ-AEWs system from an energy perspective**

15   Traditional studies have used the mid-tropospheric trough and ridge from unfiltered

16   wind fields to diagnose the AEWs. In this manner, the AEWs trough was identified where

17   the meridional wind at the vertical level of the AEJ is equal to zero, indicating that the wind

18   shifts from northerlies to southerlies (Diedhiou et al., 1999). The existence of two distinct

19   tracks of the AEWs: the northern and southern tracks (e.g., Diedhiou et al., 1999; Nitta and

20   Takayabu, 1985; Reed et al., 1988; Wu et al., 2013) have been identified by examining the

21   vorticity structure of the AEWs (e.g., Carlson 1969 a&b; Thorncroft and Hodges, 2001;

22   Hopsch et al., 2007) and applying the reversal of the meridional gradient of potential

23   vorticity (e.g., Norquist et al., 1977; Pytharoulis and Thorncroft, 1999; Kiladis et al., 2006).

1   However, these methods are limited because of the overlapping scale of AEWs with other

2   phenomena and the significant amount of manual intervention required to differentiate

3   between synoptic-scale AEW trough axes and localized circulation centers. As a solution

4   to this problem, here we applied the eddy energy budget to diagnose the growth and

5   evolution of the AEWs.

6   Hosseinpour and Wilcox (2014) showed that the axis of the AEJ core resides at

7   about 600-hPa during the boreal summer; thus, here we present the results for 600-hPa,

8   where the activity of the AEJ-AEWs system is maximized. Figure 1a shows the mid-level

9   AEJ in the climatology of boreal summer. The core of the jet is zonally located from 20°

10   E to 30° W between the Sahel and the Sahara and spans from Africa toward the Atlantic

11   Ocean, where the jet axis is located at ~15° N latitude. The closed contours in Figure 1b-c

12   represent the MKE of the AEJ. The MKE peaks at ~12-18° N, collocated with the core of

13   the AEJ (Figure 1a). The long-term mean of the mid-level EKE for the 2-6-day (warm

14   shades in Figure 1b) and 6-11-day (warm shades in Figure 1c) bandpass filtered EKE

15   represents the kinetic energy of two distinct categories of the AEWs: The 2-6-day bandpass

16   EKE peaks offshore, downstream and along the northern side of the jet core, while the 6-

17   11-day bandpass EKE has a weaker signal over the northern side of the jet compared to 2-

18   6-day EKE. The significant signal of the 2-6-day AEWs over the tropical Atlantic implies

19   the significant contribution of 2-6-day transient eddies in transient disturbances over the

20   Ocean.

21   In addition, both 2-6-day and 6-11-day bandpass EKE can develop at the higher

22   latitudes above ~32° N toward the subtropics, which can be related to the impacts of the

23   westerly Rossby waves of the subtropical storm track over North Africa. These are

1   consistent with the previous studies, showing that after leaving the West coast of Africa,

2   the majority of AEWs either (1) penetrate the subtropical Atlantic Ocean via an interaction

3   with an extratropical trough, or (2) develop further downstream and are involved in tropical

4   cyclogenesis (Berry et al., 2007; Chen et al., 2008).

5   **3.1.1   Behaviors of transient eddies of the AEWs**

6   In this Section, we further investigate the characteristics of the AEWs. Figures 1d

7   and 1e show the climatology of transient eddies. The variance of zonal wind ($\overline{u'^2}$)

8   represents the zonal transient eddies (Figure 1d), which peak at ~6-12° N and are elongated

9   downstream along the southern edge of the AEJ from approximately 15° W to 45° W.

10   Comparing this with Figure 1b shows that the increase of 2-6-day bandpass EKE

11   downstream of the jet core corresponds to the 2-6-day zonal transient eddies, whereas the

12   core of the 2-6-day EKE over the northern track AEWs at ~18-24° N is related to the

13   meridional wind variance ($\overline{v'^2}$), which represents the 2-6-day meridional transient eddies

14   (Figure 1e). These patterns suggest that transient eddies of the 2-6-day time-scale AEWs

15   are elongated both zonally and meridionally.

16   Figure 1f gives further information about the structure and propagation of the 2-6-

17   day eddies. The enhanced transient momentum flux ($\overline{u'v'}$) of 2-6-day bandpass eddies over

18   the northern and southern tracks of the AEWs indicates the orientation and the group

19   velocity of the transient eddies relative to easterly mean-flow. The positive values of the

20   transient momentum flux are dominant over the southern sides of the jet core, suggesting

21   that the southern track transient eddies propagate with a NE-SW orientation, whereas the

22   negative values of the transient momentum flux over the northern track suggest the NW-

1   SE orientation of transient eddies relative to the mean-flow. The relatively tilted

2   orientations of the eddies over the northern and southern track, fanning out or diverging

3   downstream of the jet core, are signatures of the so-called downstream development, where

4   transient eddy activity associated with 2-6-day AEWs is enhanced. The magnitude of the

5   transient momentum flux shows the 2-6-day eddies over the northern and southern tracks

6   of the AEWs propagate faster relative to the easterly mean-flow, whereas the values of

7   transient momentum flux are negligible along the AEJ axis where the mean-flow is strong.

8   To further investigate the behavior of the 2-6-day eddies, we discuss the baroclinic and

9   barotropic instability of the waves in the following Section.

10   **3.1.2   Baroclinic instability of the AEJ-AEWs system**

11   Baroclinic instability is the dynamic cause for synoptic-scale storms as a result of

12   vertical shear of the zonal wind, corresponding to meridional temperature gradients based

13   on the thermal wind balance (e.g., Charney, 1947; Eady, 1949). Meridional temperature

14   gradient is also proportional to the available potential energy in baroclinic instability

15   mechanism (Hoskins et al., 1983; Grotjahn, 2003). Baroclinic zones are defined as the

16   favored areas for strengthening and weakening of systems, where eddies extract available

17   potential energy from the mean-flow and convert the eddy available potential energy to

18   EKE through baroclinic conversion (BCC) of energy (Chang et al., 2002; Orlanski and

19   Katzfey, 1991). The changes in meridional temperature gradient also contribute to the

20   changes in EKE of the waves (e.g., Coumou et al., J., 2015; Gertler and O'Gorman, 2019).

21   Previous studies showed that $\overline{u'v'}$ is an indicator of baroclinic instability at the exit

22   region of the jet (e.g., Hoskins et al., 1983). Figure 1f represents the presence of baroclinic

1   instability ($\overline{u'v'}$) at the northern and southern tracks of the waves downstream of the jet

2   core, showing the development of the 2-6-day transient eddy activity downstream of the

3   AEJ corresponds to the presence of baroclinic instability in the region where eddies can

4   extract energy from the easterly mean-flow through baroclinic conversion (as described in

5   the following Section). These suggest that the northern and southern tracks of the AEWs

6   are favorable areas for the potential growth of baroclinic transient eddies as the variations

7   in baroclinic instability tend to extract energy from the jet and convert it to eddy energy

8   downstream of the AEJ, where the jet weakens.

9   We further investigated the conversion of energy through BCC by studying the

10   fraction of the total variance of BCC (Figure 1g) attributable to variations on less than 11-

11   day time scales, which includes both the 2-6-day AEWs and 6-11-day AEWs. Figure 1g

12   shows that these variations account for a significant fraction of BCC variations over land,

13   where the AEJ core resides (Figure 1a), and this high fraction of BCC variance extends

14   offshore over the northern and southern sides of the AEJ. This is consistent with the

15   discussion above, suggesting the eddy activity occurs at the north and south sides of the

16   AEJ (Figure 1f), where the transient zonal and meridional eddies (Figures 1d-e) extract

17   energy from the MKE (contours in Figure 1b-c) and convert it to EKE (Figure 1b-c)

18   through BCC.

19   In the next Section, we investigated the relationships between the African aerosols

20   and the AEWs. Studying the time series of EKE and dust anomalies shows a similarity

21   between the variability of dust radiative effect and the changes of the 2-6-day EKE over

22   the northern and southern tracks of the AEWs (Figures S1 and S2), suggesting a possible

23   impact of dust diabatic heating on the enhancement of the kinetic energy of the AEWs.

1   Such a relationship between dust and AEWs is also seen over each individual JJA (Figures

2   S1, S2, and S3). We explore Saharan dust variability (Section 3.2) and then investigate the

3   possible impacts of aerosol radiative effect of dust concentration on the energy of AEWs

4   (Section 3.3).

6   **3.2   Saharan dust plumes- climatology and variability**

7   The significant dust transport from the Saharan desert across the Atlantic Ocean is

8   seen in the long-term mean of Saharan dust optical thickness and radiative effect vertically

9   integrated over the troposphere during boreal summer (Figures 2a-c). The inherent

10   limitation of MODIS satellite observations is the lack of AOD data over the highly-

11   reflective desert regions (Figure 2a) and the Deep Blue AOD over the Ocean (Figure 2b).

12   Because of that, based on Eq. (1) we calculated aerosol shortwave radiative effect from the

13   MERRA-2 reanalysis as a complementary component (Figure 2c) to the satellite

14   observations. This was further examined by the scatter plots of MODIS AOD over the

15   Ocean (Figure 2d) and Deep Blue over the land (Figure 2e) with respect to MERRA-2

16   radiative effect, where daily data points were averaged over the oceanic and land dust

17   domains (rectangle in Figures 2a and 2b, respectively). This shows that MERRA-2

18   reanalysis is highly correlated with MODIS observations with R-values of 0.83 and 0.62,

19   respectively, and statistically significant with P-values less than 0.05. From a climatology

20   point of view, the maximum value of dust heating the atmosphere is approximately 35 Wm^{-2},

21   localized over the western and central Saharan Desert in JJA, 2000-2021 (Figure 2c). In

22   addition, the radiative effect efficiency for atmospheric heating by Saharan dust inferred

1   from these scatter plots (Figures 2d-e) is roughly 20 Wm^{-2} per unit AOD over the ocean

2   and 35 Wm^{-2} per unit AOD over land.

3   We investigated dust variability by studying the changes in daily radiative effect

4   during dust transport across the tropical Atlantic Ocean. The longitude-time Hovmöller

5   diagrams of daily aerosol radiative effect anomalies are provided for each summer from

6   2000 to 2021 (Figure 3). The aerosol radiative effect is meridionally averaged over the

7   SAL, 12-22°N, where the dust concentration is high. The positive and negative anomalies

8   show the increase and decrease of aerosol radiative effect within the SAL as dust

9   propagates in transient dust plumes across the tropical Atlantic Ocean. Figure 3 shows that,

10 on average, dust transport may reach the Caribbean Sea in less than 11 days. To investigate

11 the climatology of this, the fraction of total variance of dust radiative effect was calculated

12 for less than 11-day and more than 11-day of dust variations during boreal summer seasons,

13 2000-2021 (Figures 2f-g). The variations of aerosol radiative effect for less than 11-day

14 timescale variations are significant over West Africa and the eastern tropical Atlantic

15 Ocean and account for up to 70-80% of the total variance of aerosol radiative effect over

16 these regions. In contrast, the variations of dust radiative effect longer than 11-day are a

17 more significant fraction of the variance upstream, mainly over the dust sources in the

18 Saharan Desert.

19   We conducted similar Hovmöller analyses as above, but for MODIS observations

20 as a check on the variability of dust radiative effect in the MERRA-2 reanalysis and found

21 that the results from MERRA-2 reanalysis were consistent with the MODIS AOD (Figure

22 S3). Analyzing the dust storm events from 2000 to 2021 suggests a possible relationship

23 between the dust transport and the variations of the AEJ-AEWs system. Our hypothesis is

1   that the variations of dust across the ocean during Saharan dust storms contribute to the

2   growth of the waves over the ocean through diabatic heating from dust radiative effect. To

3   investigate this, we focus on the dust over the oceanic domain (i.e., OSAL; rectangle in

4   Figure 2a). The steps to study this are described in the following sections.

5   **3.3   Impacts of dust radiative effect on the energy of the AEWs**

6   Previous studies have discussed the dynamics of the AEWs as summarized in the

7   introductory Section; however, the relationships between dust radiative effect and the

8   kinetic energy of the AEWs are still unexplored. In this Section, we investigate the

9   relationships between dust radiative effect of the atmosphere (TOA minus surface) and the

10   kinetic energy of the AEWs during the boreal summer from 2000 to 2021.

11   **3.3.1   Composite analysis of eddy energetics with respect to dust variability**

12   The composite analyses were conducted for the boreal summer seasons of 22 years.

13   The composite of the 2-6-day and 6-11-day filtered EKE (Figures 4a and 4b, respectively)

14   are based on the EKE values for the times that correspond to the upper-quartile dust

15   radiative effect in the OSAL region (rectangle in Figure 2a) minus the EKE values of the

16   times correspond to the lower-quartile dust radiative effect. The steps to calculate

17   composite diagrams are explained in Section 2.

18   The positive anomalies in Figure 4a show the increase of the 2-6-day EKE at the

19   southern track (~ 6-12°N) of the AEWs and further downstream over the northern track (~

20   18-24°N) coincide with the enhanced radiative effect of dust over the offshore region. The

21   dipole pattern of the positive and negative anomalies may also imply a possible southward

1   shift of the 2-6-day EKE at the southern edge of the AEJ during high dust concentrations.

2   A similar dipole pattern can also be seen in Figure 4c.

3   Figure 4c shows the increase of the zonally elongated 2-6-day eddies at the southern

4   edge of the jet, which suggests that the strengthening of the 2-6-day zonal transient eddies

5   may lead to the amplification of EKE (Figure 4a) over the southern track of the waves

6   during dust events when aerosol radiative effect is significant offshore. Meanwhile, the

7   increase of the meridional elongated transient eddies (Figure 4d) coincides with the high

8   concentrations of dust. Comparing this with Figure 4a suggests that during high dust

9   concentration in OSAL, the amplification of the 2-6-day EKE further downstream in the

10   northern track of the AEWs corresponds to the enhanced meridional elongated transient

11   eddies. While the positive anomalies of 2-6-day $\overline{u'v'}$ (Figure 4e) is a weaker signal at the

12   northern and southern tracks of the waves, it is still statistically significant, which shows

13   that the enhancement of the baroclinic instability over the northern and southern tracks of

14   the AEWs occurs during high aerosol radiative effect in OSAL.

15   The negative composite along the AEJ axis at about 12-18°N (Figure 4) can be

16   related to the fact that the 2-6-day and 6-11-day EKE are not significant along the AEJ

17   axis, where the MKE and the horizontal shear of mean-flow are strong (Figure 1a-b-c). As

18   described in Section 3.1., the growth of transient eddies is more likely over the south and

19   north side of the jet, where the jet weakens and thus offers a greater chance for the

20   development of baroclinic AEWs (Figure 1f-g). While the negative anomaly may seem

21   like a reduction of eddy activity along the AEJ axis simultaneously at the time of dust

22   enhancement, in the next Section (3.3.2), we have evidence that the amplification of 2-6-

1   day EKE along the AEJ axis starts on average two days after the peak of dust offshore

2   (Figures 5 d-e).

3   We conducted the same composite analysis using MODIS AOD, which shows that

4   the results are consistent whether the MERRA-2 radiative effect metric or the MODIS

5   AOD data are applied (Figure S4). Overall, these composite analyses suggest a mechanistic

6   relationship between the kinetic energy of the AEJ-AEWs system over the ocean and

7   aerosol radiative effect during dust outbreaks in summer. The enhanced dust offshore

8   coincides with the strengthening of the baroclinic instability and amplification of the 2-6-

9   day AEWs downstream, where the jet weakens and gives a chance to strengthen the

10   propagation of the zonally and meridionally elongated transient eddies over the southern

11   and northern tracks of the waves, respectively. In the following Section, we study a possible

12   time lag between the occurrence of dust storms and the changes in the activity of the waves

13   over various domains.

15   **3.3.2   Time-lag between dust outbreaks and development of the AEWs**

16   In this Section, we investigate a possible lag between the changes of the EKE with

17   respect to the variability of dust radiative effect over the OSAL. We divide the northern

18   track waves (18° to 24° N) and southern track (6° to 12° N) of the AEWs into two separate

19   regions: Eastern Atlantic (-15° to -30°E) and Central Atlantic (-30° to -45°E). We also

20   study the possible lag between dust in OSAL and the eddy activity downstream of the jet

21   core (12° to 18°N) over the eastern and central Atlantic domains (Table 2). The time lag is

22   investigated between composite EKE over each wave domain with respect to composite

1   dust radiative effect in OSAL. The methodology for calculating time lag is described in

2   Section 2.

3   The variability of dust radiative effect (i.e., composite for daily upper quartile

4   aerosol radiative effect minus daily lower quartile aerosol radiative effect) in Figure 5a

5   represents the daily variations of radiative effect five days before and after the peak of dust

6   in the OSAL region for the 22 years of boreal summer seasons. This shows the variability

7   of dust radiative effect associated with the dust outbreaks over the OSAL region is

8   significant for about six days, as it starts three days before (T = -3) and ends three days

9   after (T = +3) the peak of dust (T = 0), which is consistent with the timescale of the 2-6-

10 day AEWs. Similar analyses are conducted using the upper quartile radiative effect only to

11 investigate such relationships for the days with high dust concentration (Figure S5). The

12 results are consistent with the patterns shown in Figure 5.

13   Figures 5b represents the time evolution and changes in 2-6-day EKE of the

14 northern track AEWs further downstream over the eastern Atlantic Ocean. The changes in

15 EKE seem negligible at T < 0 before starting the high variations in dust in OSAL; however,

16 the growth of EKE occurs on average at T = 0, coinciding with the peak of dust, and then

17 continues growing and reaches its maximum about three days (T = +3) after the peak of

18 dust variations. In contrast, although a slight decrease and increase of EKE are seen

19 respectively before and after dust peaks, the variations of the northern track EKE over the

20 eastern Atlantic (Figure 5c) seem weaker compared to those further downstream.

21 Comparing Figure 5b with the composite analysis in Figure 4a suggests that the

22 enhancement of the northern track 2-6-day EKE, further downstream over the central

1   Atlantic, coincides with the peak of dust and is even more significant on average three days

2   after dust peaks in OSAL.

3   The negative variations of the EKE in Figures 5d and 5e at T = 0 are consistent with

4   the negative composite of the EKE along the AEJ axis in Figure 4. This means that the

5   decay of EKE along the jet axis over the Central Atlantic (Figure 5d) is initiated before

6   dust activity; however, the rapid growth of EKE starts on average two days (T = +2) after

7   the peak of dust and is maximized about three to four days (T ~ +3 to +4) after the peak of

8   dust in OSAL. A similar, but weaker pattern, is seen across the jet axis over the eastern

9   Atlantic (Figure 5e).

10   Figures 5f and 5g show that the changes in EKE are maintained positive before and

11   after dust activity. Comparing Figure 5f with Figure 5a suggests that the activity of both

12   dust plumes in OSAL and the southern EKE anomalies over the central Atlantic is initiated

13   about three days (T = -3) before dust peaks, and then amplification of EKE continues and

14   reaches its maximum on average two days (T = +2) after dust peaks.

15   Over the eastern tropical Atlantic (Figure 5g), the EKE variations seem negligible

16   during dust storms. The weaker signal of the southern track EKE variations over the eastern

17   Atlantic can be explained by the dynamic and energy of the AEJ-AEWs system (Figure 1),

18   as this is the region where the southern edge of the jet is dominant, and the MKE and

19   conversion of energy to EKE through BCC are significant. This suggests that while the

20   positive anomalies of EKE over this region coincide with the enhancement of dust in

21   OSAL, the influence of dust radiative effect on changes in EKE could be weak

22   quantitatively compared to the amount of energy exchange between the components of the

23   AEJ-AEWs system at the southern edge of the jet core.

1   Comparing Figures 5b, 5d, and 5f reveals evidence of the mechanistic relationship

2   between variability of dust radiative effect offshore and the changes in the 2-6-day EKE

3   further downstream over the Central tropical Atlantic, where the easterly flow weakens at

4   the exit region of the jet over the central Atlantic. On average, the peak of dust load in

5   OSAL occurs a few days before the amplification of the EKE downstream of the AEJ; a

6   similar pattern is also seen with a weaker signal over the eastern tropical Atlantic. The lag

7   analyses, summarized in Table 3, suggest that the peak of dust aerosols loading offshore

8   over the OSAL region precedes the amplification of EKE further downstream of the AEJ

9   over the central Atlantic Ocean. This evidence is consistent with our hypothesis on the

10   influence of dust radiative effect, fueling the EKE of the 2-6-day AEWs downstream of the

11   AEJ over the tropical Atlantic Ocean, where tropical cyclogenesis and hurricane activity

12   occur. We further investigated our analyses by selecting various dust domains (e.g., 12° to

13   22°N and -38° to -28°E, shown in Figure S6) and showed that our findings are consistent

14   regardless of the location of dust domain in SAL across the tropical Atlantic Ocean.

16   **4   Conclusions**

17   While previous studies showed the relationship between dust transport and AEJ and

18   AEWs across the Atlantic Ocean (Perry et al., 1997; Liu et al., 2008; Francis et al., 2020;

19   Francis et al., 2021) the feedback of dust to AEJ-AEW is not well understood. A few recent

20   studies showed that dust affects the atmospheric dynamics of the Atlantic Ocean by

21   enhancing AEJ and AEW strength (e.g., Bercos-Hickey et al., 2017; Grogan et al., 2016).

22   However, the mechanisms of such effects are still open questions.

1   This study shows mechanistic relationships between the radiative effect of dust

2   aerosols in SAL and the kinetic energy of the AEWs across the tropical Atlantic Ocean

3   using 22 years of daily satellite observations, as well as reanalysis data based on satellite

4   assimilation. Dust plumes across the Atlantic are not merely transported by AEJ-AEWs

5   system but also contribute to increasing the kinetic energy of the baroclinic AEWs through

6   diabatic heating. The enhanced dust contributes to an increase in meridional temperature

7   gradients (Hosseinpour and Wilcox, 2014), which leads to an increase in baroclinicity and

8   amplification of the EKE of the AEWs.

9   The efficiency of dust radiative effect in the atmosphere is a heating of roughly 20

10   Wm^{-2} per unit AOD over the ocean and 35 Wm^{-2} per unit AOD over land. This agrees with

11   in-situ measurements (Soupiona et al., 2020) and regional climate modeling (Saidou

12   Chaibou et al., 2020) of Saharan dust radiative effect. This radiative effect of dust aerosols

13   in the SAL contributes to the diabatic heating of the atmosphere in the regions

14   (Hosseinpour and Wilcox, 2014) where the increase in temperature gradients leads to the

15   growth of baroclinic waves through the conversion of energy to EKE in the AEJ-AEWs

16   system. Outbreaks of high dust concentrations in the SAL coincide with the growth of the

17   meridionally elongated 2-6-day transient eddies over the northern track of AEWs (~18-

18   24°N) and zonally elongated eddies over the southern track of AEWs (~6-12°N). This leads

19   to amplifying the EKE of the AEWs, particularly at the exit region of the AEJ, where the

20   MKE and the horizontal shear of mean-flow are weakened. This offers the chance for

21   downstream development of the AEWs, associated with enhanced dust. The dust-induced

22   enhancement of AEW through a buoyancy source was shown by Grogan et al. (2016),

23   albeit with a different methodology (i.e., analytical and regional modeling analyses). In

1   addition, our results agree with a case study of the Saharan dust event by a regional climate

2   model (Bercos-Hickey et al., 2017) that showed that Saharan dust causes AEW to shift

3   northward and expand westward.

4   The growth of the baroclinic transient eddies, and the corresponding EKE of the 2-

5   6-day AEWs, is amplified at the exit region of the AEJ, on average, two to four days after

6   the enhancement of dust upstream in the OSAL region. Our findings show that dust activity

7   precedes the amplification of EKE, suggesting that the diabatic heating from dust radiative

8   effect can fuel the development of the AEWs. This mechanistic impact of dust radiative

9   effect onto AEW development is consistent across the tropical Atlantic Ocean.

10   This study further supports a hypothesis between dust radiative effect and transient

11   wave dynamics that may be tested in sensitivity studies with dynamical climate models to

12   explore further the cause and effect of such relationships. The data assimilation in

13   MERRA-2 provides a realistic representation of circulation, while one caveat of using

14   MERRA-2 alone is that it is not possible to compare a dust-free circulation to a dusty

15   circulation. The empirical relationships apparent from this study will be examined in a

16   follow-on study of atmospheric general circulation model simulations with and without the

17   dust radiative effect to further explore the hypothesis linking dust radiative effects to AEW

18   dynamics.

20   **Acknowledgments**

21   This work is supported by the NASA Interdisciplinary Science Program through grants

22   #NNX11AF21G and #NNX14AH95G. Special thanks to Drs. Peter Colarco, Naresh

23   Kumar, and Hans Moosmuller for their constructive comments that contributed to the

1 improvement of this manuscript. We also appreciate the anonymous reviewers for their

2 constructive comments.

Data availability

5 MERRA-2 aerosol, radiation, and meteorological datasets can be obtained from

6 https://disc.gsfc.nasa.gov/datasets. MODIS AOD retrievals are accessible through

7 https://modis.gsfc.nasa.gov/data/dataprod/mod04.php. Numerical codes developed to

8 conduct data extraction, analysis, and visualization will be provided upon request.

Author contributions

12 FH and EW originated this study. FH formulated, developed and implemented the codes,

13 and analyzed the results. FH drafted and finalized the paper, and EW provided edits and

14 revisions.

Competing interests

17 The authors have no competing interests.

References

20 Avila, L. A. and Clark, G. B.: Atlantic Tropical Systems of 1988, Mon. Wea. Rev., 117,
21 2260-2265, https://doi.org/10.1175/1520-0493(1989)117%3C2260:ATSO%3E2.0.CO;2,
22 1989.

23 Avila, L. A. and Pasch, R. J.: Atlantic Tropical Systems of 1991, Mon. Wea. Rev., 120,
24 2688-2696, https://doi.org/10.1175/1520-0493(1992)120, 1992.

1 Barbosa, P. M., Stroppiana, D., Grégoire, J. M., and Cardoso Pereira, J. M.: An
2 assessment of vegetation fire in Africa (1981–1991): Burned areas, burned biomass, and
3 atmospheric emissions, Global Biogeochem. Cy., 13, 933-950,
4 https://doi.org/10.1175/1520-0493(1992)120, 1999.

5 Bercos-Hickey, E. and Patricola, C. M.: Anthropogenic influences on the African easterly
6 jet–African easterly wave system, Clim. Dyn., 57, 2779–2792,
7 https://doi.org/10.1007/s00382-021-05838-1, 2021.

8 Bercos-Hickey, E., Nathan, T. R., and Chen, S. H.: Saharan dust and the African easterly
9 jet-African easterly wave system: Structure, location and energetics, Q. J. Roy. Meteor.
10 Soc., 143, 2797–2808, https://doi.org/10.1002/qj.3128, 2017.

11 Bercos-Hickey, E., Nathan, T. R., and Chen, S.-H.: On the Relationship between the
12 African Easterly Jet, Saharan Mineral Dust Aerosols, and West African Precipitation, J.
13 Clim., 33, 3533-3546, https://doi.org/10.1175/jcli-d-18-0661.1, 2020.

14 Berry, G. J. and Thorncroft, C. D.: African easterly wave dynamics in a mesoscale
15 numerical model: The upscale role of convection, J. Atmos. Sci., 69, 1267-1283,
16 https://doi.org/10.1175/JAS-D-11-099.1., 2012.

17 Berry, G. J., Thorncroft, C. D., and Hewson, T.: African easterly waves during 2004—
18 Analysis using objective techniques, Mon. Wea. Rev., 135, 1251-1267,
19 https://doi.org/10.1175/MWR3343.1, 2007.

20 Buchard, V., Randles, C. A., da Silva, A. M., Darmenov, A., Colarco, P. R., and
21 Govindaraju, R.: The MERRA-2 Aerosol Reanalysis, 1980 Onward. Part II: Evaluation
22 and Case Studies, J. Clim., 30, 6851-6872, https://doi.org/10.1175/JCLI-D-16-0613.1,
23 2017.

24 Cahoon, D. R., Stocks, B. J., Levine, J. S., Cofer, W. R., and O'Neill, K. P.: Seasonal
25 distribution of African savanna fires, Nature, 359, 812-815,
26 https://doi.org/10.1038/359812a0, 1992.

27 Carlson, T. N.: Synoptic histories of three African disturbances that developed into
28 Atlantic hurricanes, Mon. Wea. Rev., 97, 256–276, https://doi.org/10.1175/1520-
29 0493(1969)097%3C0256:SHOTAD%3E2.3.CO;2, 1969.

30 Carlson, T. N. and Prospero, J. M.: The Large-Scale Movement of Saharan Air Outbreaks
31 over the Northern Equatorial Atlantic, J. Appl. Meteorol., 11, 283–297,
32 https://doi.org/10.1175/1520-0450(1972)011<0283:TLSMOS>2.0.CO;2, 1972.

33 Chang, C. B.: Impact of desert environment on the genesis of African wave disturbances,
34 J. Atmos. Sci., 50, 2137–2145, https://doi.org/10.1175/1520-
35 0469(1993)050%3C2137:IODEOT%3E2.0.CO;2, 1993.

36 Chang, E. K. M., Lee, S., and Swanson, K. L.: Storm track dynamics, J. Clim., 15, 2163-

2183, https://doi.org/10.1175/1520-0442(2002)015, 2002.

Charney, J. G.: The Dynamics of Long Waves in a Baroclinic Westerly Current, J. Atmos. Sci., 4, 136–162, https://doi.org/10.1175/1520-0469(1947)004%3C0136:TDOLWI%3E2.0.CO;2, 1947.

Charney, J. G. and Stern, M. E.: On the stability of internal baroclinic jets in a rotating atmosphere, J. Atmos. Sci., 19, 159–172, https://doi.org/10.1175/1520-0469(1962)019%3C0159:OTSOIB%3E2.0.CO;2, 1962.

Chen, S. H., McDowell, B., Huang, C. C., and Nathan, T. R.: Formation of a low-level barrier jet and its modulation by dust radiative forcing over the Hexi Corridor in Central China on March 17, 2010, Q. J. Roy. Meteor. Soc., 147, 1873–1891, https://doi.org/10.1002/qj.4000, 2021.

Chen, T., Wang, S., and Clark, A. J.: North Atlantic Hurricanes Contributed by African Easterly Waves North and South of the African Easterly Jet, J. Clim., 21, 6767-6776, https://doi.org/10.1175/2008JCLI2523.1, 2008.

Cochrane, S. P., Schmidt, K. S., Chen, H., Pilewskie, P., Kittelman, S., Redemann, J., LeBlanc, S., Pistone, K., Segal Rozenhaimer, M., Kacenelenbogen, M., Shinozuka, Y., Flynn, C., Ferrare, R., Burton, S., Hostetler, C., Mallet, M., and Zuidema, P.: Biomass burning aerosol heating rates from the ORACLES (ObseRvations of Aerosols above CLouds and their intEractionS) 2016 and 2017 experiments, Atmos. Meas. Tech., 15, 61-77, https://doi.org/10.5194/amt-15-61-2022, n.d.

Colarco, P. R., Toon, O. B., and Holben, B. N.: Saharan dust transport to the Caribbean during PRIDE: 1. Influence of dust sources and removal mechanisms on the timing and magnitude of downwind aerosol optical depth events from simulations of in situ and remote sensing observations, J. Geophys. Res. Atmos., 108, 8589, https://doi.org/10.1029/2002JD002658., 2003.

Colarco, P. R., Silva, A., Chin, M., and Diehl, T.: Online simulations of global aerosol distributions in the NASA GEOS-4 model and comparisons to satellite and ground-based aerosol optical depth, J. Geophys. Res. Atmos., 115, D14207, https://doi.org/10.1029/2009JD012820., 2010.

Cornforth, R. J., Hoskins, B. J., and Thorncroft, C. D.: The impact of moist processes on the African easterly jet–African easterly wave system Q, J. R. Meteorol. Soc, 135, 894-913, https://doi.org/10.1002/qj.414., 2009.

Coumou, D., Lehmann, J., and Beckmann, J.: The weakening summer circulation in the Northern Hemisphere mid-latitudes, Science, 348, 324–327, https://doi.org/10.1126/science.1261768, 2015.

Dee, D. P.: The ERA-Interim reanalysis: configuration and performance of the data

assimilation system, Q. J. R. Meteorol. Soc., 137, 553–597, https://doi.org/10.1002/qj.828, 2011.

Diaz, M. and Aiyyer, A.: The Genesis of African Easterly Waves by Upstream Development, J. Atmos. Sci., 70, 3492–3512, https://doi.org/10.1175/JAS-D-12-0342.1, 2013.

Diedhiou, A.: Easterly wave regimes and associated convection over West Africa and tropical Atlantic: results from the NCEP/NCAR and ECMWF reanalyses, Clim. Dyn., 15, 795-822, https://doi.org/10.1007/s003820050316, 1999.

Duchon, C. E.: Lanczos filtering in one and two dimensions, J. Appl. Meteorol., 18, 1016-1022, https://doi.org/10.1175/1520-0450(1979)018, 1979.

Dunn, G. E.: Cyclogenesis in the tropical Atlantic, Bull. Amer. Meteor. Soc., 21, 215–229, https://doi.org/10.1175/1520-0477-21.6.215, 1940.

Eady, E. T.: Long Waves and Cyclone Waves, Tellus, 1, 33–52, https://doi.org/10.1111/j.2153-3490.1949.tb01265.x, 1949.

Francis, D., Fonseca, R., Nelli, N., Cuesta, J., Weston, M., Evan, A., and Temimi, M.: The atmospheric drivers of the major Saharan dust storm in June 2020, Geophys. Res. Lett., 47, e2020GL090102, https://doi.org/10.1029/2020GL090102, 2020.

Francis, D., Nelli, N., Fonseca, R., Weston, M., Flamant, C., and Cherif, C.: The dust load and radiative impact associated with the June 2020 historical Saharan dust storm, Atmos. Environ., 268, 118808, https://doi.org/10.1016/j.atmosenv.2021.118808, 2022.

Gelaro, R., McCarty, W., Suárez, M. J., Todling, R., Molod, A., and Takacs, L.: The modern-era retrospective analysis for research and applications, version 2 (MERRA-2), J. Clim., 30, 5419–5454, https://doi.org/10.1175/JCLI-D-16-0758.1, 2017.

Gertler, C. G. and O'Gorman, P. A.: Changing available energy for extratropical cyclones and associated convection in Northern Hemisphere summer, P. Natl. Acad. Sci., 116, 4105–4110, https://doi.org/10.1073/pnas.1812312116, 2019.

Global Modeling and Assimilation Office (GMAO): MERRA-2 inst3_3d_asm_Np: 3d,3-Hourly,Instantaneous,Pressure-Level,Assimilation,Assimilated Meteorological Fields V5.12.4, Greenbelt, MD, USA, Goddard Earth Sciences Data and Information Services Center (GES DISC)[Dataset], https://doi.org/10.5067/QBZ6MG944HW0, 2015c.

Global Modeling and Assimilation Office (GMAO): MERRA-2 inst6_3d_ana_Np: 3d,6-Hourly,Instantaneous,Pressure-Level,Analysis,Analyzed Meteorological Fields V5.12.4, Greenbelt, MD, USA, Goddard Earth Sciences Data and Information Services Center (GES DISC)[Dataset], https://doi.org/10.5067/A7S6XP56VZWS, 2015a.

Global Modeling and Assimilation Office (GMAO): MERRA-2 tavg1_2d_rad_Nx: 2d,1-

Hourly,Time-Averaged,Single-Level,Assimilation,Radiation Diagnostics V5.12.4, Greenbelt, MD, USA, Goddard Earth Sciences Data and Information Services Center (GES DISC)[Dataset], https://doi.org/10.5067/Q9QMY5PBNV1T, 2015b.

Grogan, D. F., Nathan, T. R., and Chen, S. H.: Effects of Saharan dust on the linear dynamics of African easterly waves, J. Atmos. Sci., 73, 891–911, https://doi.org/10.1175/JAS-D-15-0143.1, 2016.

Grogan, D. F., Nathan, T. R., and Chen, S. H.: Structural changes in the African easterly jet and its role in mediating the effects of Saharan dust on the linear dynamics of African easterly waves, J. Atmos. Sci., 76, 3351–3365, https://doi.org/10.1175/JAS-D-19-0104.1, 2019.

Grogan, D. F. P., Lu, C.-H., Wei, S.-W., and Chen, S.-P.: Investigating the impact of Saharan dust aerosols on analyses and forecasts of African easterly waves by constraining aerosol effects in radiance data assimilation, Atmos. Chem. Phys., 22, 2385-2398, https://doi.org/10.5194/acp-22-2385-2022., 2022.

Grotjahn, R.: Baroclinic instability, Enc. Atmos. Sci., 419, 467, https://doi.org/10.1016/B0-12-227090-8/00076-2, 2003.

Haarig, M., Walser, A., Ansmann, A., Dollner, M., Althausen, D., and Sauer, D.: Profiles of cloud condensation nuclei, dust mass concentration, and ice-nucleating-particle-relevant aerosol properties in the saharan air layer over barbados from polarization lidar and airborne in situ measurements, Atmos. Chem. Phys., 19, 13773–13788, https://doi.org/10.5194/acp-19-13773-2019, 2019.

Haywood, J. M., Pelon, J., Formenti, P., Bharmal, N., Brooks, M., Capes, G., and Tulet, P.: Overview of the dust and biomass-burning experiment and African monsoon multidisciplinary analysis special observing period-0, J. Geophys. Res. Atmos., 113, https://doi.org/10.1029/2008JD010077, 2008.

Hinkelman, L. M.: The Global Radiative Energy Budget in MERRA and MERRA-2: Evaluation with Respect to CERES EBAF Data, J. Clim., 32, 1973-1994, https://doi.org/10.1175/JCLI-D-18-0445.1, 2019.

Hopsch, S. B., Thorncroft, C. D., Hodge, K., and Aiyyer, A.: West African storm tracks and their relationship to Atlantic tropical cyclones, J. Clim., 20, 2468–2483, https://doi.org/10.1175/JCLI4139.1, 2007.

Hoskins, B. J., James, I. N., and White, G. H.: The Shape, Propagation and Mean-Flow Interaction of Large-Scale Weather Systems, J. Atmos. Sci., 40, 1595-1612, https://doi.org/10.1175/1520-0469(1983)040, 1983.

Hosseinpour, F. and Wilcox, E. M.: Aerosol interactions with African/Atlantic climate dynamics, Env. Res. Let., 9, https://doi.org/10.1088/1748-9326/9/7/075004., 2014.

Hsieh, J. S. and Cook, K. H.: Generation of African Easterly Wave Disturbances: Relationship to the African Easterly Jet, Mon. Wea. Rev., 133, 1311-1327, https://doi.org/10.1175/MWR2916.1, 2005.

Hsieh, J. S. and Cook, K. H.: A Study of the Energetics of African Easterly Waves Using a Regional Climate Model, J. Atmos. Sci., 64, 421-440, https://doi.org/10.1175/JAS3851.1, 2007.

Hsu, N. C., Lee, J., Sayer, A. M., Kim, W., Bettenhausen, C., and Tsay, S. C.: VIIRS Deep Blue aerosol products over land: Extending the EOS long-term aerosol data records, J. Geophys. Res. Atmos., 124, 4026–4053, https://doi.org/10.1029/2018JD029688, 2019.

Jones, C., Mahowald, N., and Luo, C.: The role of easterly waves on African Desert dust transport, J. Clim., 16, 3617-3628, https://doi.org/10.1175/1520-0442(2003)016, 2003.

Jones, C., Mahowald, N., and Luo, C.: Observational evidence of African Desert dust intensification of easterly waves, Geophys. Res. Lett, 31, L17208, https://doi.org/10.1029/2004gl020107., 2004.

Kiladis, G. N., Thorncroft, C. D., and Hall, N. M. J.: Three-dimensional structure and dynamics of African easterly waves part I: Observations, J. Atmos. Sci., 63, 2212-2230, https://doi.org/10.1175/JAS3741.1, 2006.

Kim, K. M., Lau, W. K. M., Sud, Y. C., and Walker, G. K.: Influence of Aerosol-Radiative forcing on the diurnal and seasonal cycles of rainfall over West Africa and eastern Atlantic Ocean using GCM simulations, Clim. Dyn., 35, 115–126, 10 1007 00382-010-0750–1, https://doi.org/10.1007/s00382-010-0750-1, 2010.

Konare, A., Zakey, A. S., Solmon, F., Giorgi, F., Rauscher, S., Ibrah, S., and Bi, X. J. J. O. G. R. A.: A regional climate modeling study of the effect of desert dust on the West African monsoon, J. Geophys. Res. Atmos., 113, https://doi.org/10.1029/2007JD009322, 2008.

Lau, K. M. and Kim, K. M.: Cooling of the Atlantic by Saharan dust, Geophys, Res. Lett, 34, L23811, https://doi.org/10.1029/2007GL031538., 2007.

Lau, K. M., Kim, K. M., Sud, Y. C., and Walker, G. K.: A GCM study of the response of the atmospheric water cycle of West Africa and the Atlantic to Saharan dust radiative forcing Ann, Geophys. Res. Lett., 27, 4023-4037, https://doi.org/10.5194/angeo-27-4023-2009., 2009.

Liang, J., Chen, Y., Arellano, A. F., and Mamun, A. A.: Model sensitivity study of the direct radiative impact of saharan dust on the early stage of hurricane earl, Atmosphere, 12, 1181, https://doi.org/10.3390/atmos12091181, 2021.

Liu, D., Wang, Z., Liu, Z., Winker, D., and Trepte, C.: A height resolved global view of

dust aerosols from the first year CALIPSO lidar measurements, J. Geophys. Res. Atmos., 113, D16214, https://doi.org/10.1029/2007JD009776., 2008.

Lorenz, E. N.: Available potential energy and the maintenance of the general circulation, Tellus, 7, 157-167, https://doi.org/10.1111/j.2153-3490.1955.tb01148.x., 1955.

Ma, P. L., Zhang, K., Shi, J. J., Matsui, T., and Arking, A.: Direct radiative effect of mineral dust on the development of African easterly waves in late summer 2003–07, J. Appl. Meteorol. Clim., 51, https://doi.org/10.1175/JAMC-D-11-0215.1., 2012.

Mamun, A., Chen, Y., and Liang, J.: Radiative and cloud microphysical effects of the Saharan dust simulated by the WRF-Chem model, J. Atmos. Sol.-Terr. Phys., 219, 105646, https://doi.org/10.1016/j.jastp.2021.105646, 2021.

Matsuki, A., Quennehen, B., Schwarzenboeck, A., Crumeyrolle, S., Venzac, H., Laj, P., and Gomes, L.: Temporal and vertical variations of aerosol physical and chemical properties over West Africa: AMMA aircraft campaign in summer 2006, Atmos. Chem. Phys., 10, 8437-8451, https://doi.org/10.5194/acp-10-8437-2010, 2010.

Mekonnen, A., Thorncroft, C. D., and Aiyyer, A. R.: Analysis of Convection and Its Association with African Easterly Waves, J. Clim., 19, 5405-5421, https://doi.org/10.1175/JCLI3920.1, 2006.

Meloni, D., Sarra, A., Brogniez, G., Denjean, C., Silvestri, L., Iorio, T., Formenti, P., Gómez-Amo, J. L., Gröbner, J., Kouremeti, N., Liuzzi, G., Mallet, M., Pace, G., and Sferlazzo, D. M.: Determining the infrared radiative effects of Saharan dust: a radiative transfer modelling study based on vertically resolved measurements at Lampedusa, Atmos. Chem. Phys., 18, 4377-4401, https://doi.org/10.5194/acp-18-4377-2018, 2018.

Ming, Y. and Ramaswamy, V.: A model investigation of aerosol-induced changes in tropical circulation, J. Clim., 24, 5125-5133, https://doi.org/10.1175/2011JCLI4108.1., 2011.

Myhre, G.: Intercomparison of satellite retrieved aerosol optical depth over the ocean, J. Atmos. Sci., 61, 499–513, https://doi.org/10.1175/1520-0469(2004)061%3C0499:IOSRAO%3E2.0.CO;2, 2004.

Nitta, T. and Takayabu, Y.: Global analysis of the lower tropospheric disturbances in the tropics during the northern summer of FGGE year. Part II: Regional characteristics of the disturbances, Pure Appl. Geophys, 123, 272–292, https://doi.org/10.1007/BF00877023, 1985.

Norquist, D. C., Recker, E., and Reed, R. J.: The energetics of African wave disturbances as observed during the phase III of GATE, Mon. Weather Rev., 105, 334-342, https://doi.org/10.1175/1520-0493(1977)105, 1977.

Orlanski, I. and Katzfey, J.: The life cycle of a cyclone wave in the Southern Hemisphere,

Part I: Eddy energy budget., J. Atmos. Sci., 48, 1972-1998, https://doi.org/10.1175/1520-0469(1991)048, 1991.

Pasch, R. J. and Avila, L. A.: Atlantic Tropical Systems of 1992, Mon. Wea. Rev., 122, 539-548, https://doi.org/10.1175/1520-0493(1994)122, 1994.

Perry, K. D., Cahill, T. A., Eldred, R. A., Dutcher, D. D., and Gill, T. E.: Long-range transport of North African dust to the eastern United States, J. Geophys. Res. Atmos., 102, 11,225-11,238, https://doi.org/10.1029/97JD00260, 1997.

Platnick, S.: MODIS Atmosphere L3 Daily Product, NASA MODIS Adaptive Processing System, Goddard Space Flight Center, USA, https://doi.org/10.5067/MODIS/MOD08_D3.061, 2015.

Plumb, R. A.: A new look at the energy cycle, J. Atmos. Sci., 40, 1669-1688, https://doi.org/10.1175/1520-0469(1983)040, 1983.

Prospero, J. M. and Lamb, P. J.: African Droughts and Dust Transport to the Caribbean: Climate Change Implications, Science, 302, 1024–1027, https://doi.org/10.1126/science.1089915, 2003.

Pytharoulis, I. and Thorncroft, C.: The low-level structure of African easterly waves in 1995, Mon. Wea. Rev., 127, 2266–2280, https://doi.org/10.1175/1520-0493(1999)127%3C2266:TLLSOA%3E2.0.CO;2, 1999.

Ramo, R., Roteta, E., Bistinas, I., Wees, D., Bastarrika, A., Chuvieco, E., and Werf, G. R.: African burned area and fire carbon emissions are strongly impacted by small fires undetected by coarse resolution satellite data, P. Natl. Acad. Sci., 118, 2011160118, https://doi.org/10.1073/pnas.2011160118, 2021.

Randles, C. A., Da Silva, A. M., Buchard, V., Colarco, P. R., Darmenov, A., Govindaraju, R., and et al.: The MERRA-2 Aerosol Reanalysis, 1980 Onward. Part I: System Description and Data Assimilation Evaluation, J. Clim., 30, 6823-6850, https://doi.org/10.1175/JCLI-D-16-0609.1, 2017.

Reale, O., Achuthavarier, D., Fuentes, M., Putman, W. M., and Partyka, G.: Tropical Cyclones in the 7-km NASA Global Nature Run for Use in Observing System Simulation Experiments, J. Atmos. Ocean. Tech., 34, 73-100, https://doi.org/10.1175/JTECH-D-16-0094.1, 2017.

Redemann, J., Wood, R., Zuidema, P., Doherty, S. J., Luna, B., LeBlanc, S. E., and et al.: An overview of the ORACLES (ObseRvations of Aerosols above CLouds and their intEractionS) project: aerosol–cloud–radiation interactions in the southeast Atlantic basin, Atmos. Chem. Phys., 21, 1507–1563, https://doi.org/10.5194/acp-21-1507-2021, 2021.

Reed, R. J., Hollingsworth, A., Heckley, W. A., Delsol, F., and L, W. U. E. T. A.: An

evaluation of the performance of the ECMWF operational system in analyzing and forecasting easterly wave disturbances 15 SEPTEMBER 2013, Mon. Wea. Rev., 116, 824–865, https://doi.org/10.1175/1520-0493(1988)116%3C0824:AEOTPO%3E2.0.CO;2, 1988.

Remer, L. A., Levy, R. C., Mattoo, S., Tanré, D., Gupta, P., Shi, Y., and Holben, B. N.: The dark target algorithm for observing the global aerosol system: Past, present, and future, Remote sensing, 12, 2900, https://doi.org/10.3390/rs12182900., 2020.

Rienecker, M. M., Suarez, M. J., Todling, R., Bacmeister, J., Takacs, L., and Liu, H. C.: The GEOS-5 Data Assimilation System—Documentation of versions 5.0.1 and 5.1.0, and 5.2.0., NASA Tech. Rep. Series on Global Modeling and Data Assimilation, NASA/TM-2008-104606, Vol. 27, 92 pp, 2008.

Rienecker, M. M., Suarez, M., Gelaro, R., Todling, R., Bacmeister, J., Liu, E., and Bosilovich, M.: MERRA: NASA's Modern-Era retrospective analysis for research and applications, J. Clim., 24, 3624-3648, https://doi.org/10.1175/JCLI-D-11-00015.1., 2011.

Roundy, P. E. and Frank, W. M.: A climatology of waves in the equatorial region, J. Atmos. Sci., 61, 2105–2032, https://doi.org/10.1175/1520-0469(2004)061, 2004.

Russell, J. O., Aiyyer, A., and Dylan White, J.: African Easterly Wave Dynamics in Convection-Permitting Simulations: Rotational Stratiform Instability as a Conceptual Model, J. Adv. Model. Earth Sys., 12, 2019 001706, https://doi.org/10.1029/2019MS001706, 2020.

Saidou Chaibou, A. A., Ma, X., and Sha, T.: Dust radiative forcing and its impact on surface energy budget over West Africa, Sci. Rep., 10, 12236, https://doi.org/10.1038/s41598-020-69223-4, 2020.

Sayer, A. M., Hsu, N. C., Lee, J., Kim, W. V., and Dutcher, S. T.: Validation, stability, and consistency of MODIS Collection 6.1 and VIIRS Version 1 Deep Blue aerosol data over land, J. Geophys. Res. Atmos., 124, 4658–4688, https://doi.org/10.1029/2018JD029598, 2019.

Soupiona, O., Papayannis, A., Kokkalis, P., Foskinis, R., Sánchez Hernández, G., Ortiz-Amezcua, P., Mylonaki, M., Papanikolaou, C.-A., Papagiannopoulos, N., Samaras, S., Groß, S., Mamouri, R.-E., Alados-Arboledas, L., Amodeo, A., and Psiloglou, B.: EARLINET observations of Saharan dust intrusions over the northern Mediterranean region (2014–2017): properties and impact on radiative forcing, Atmos. Chem. Phys, 20, 15147-15166, https://doi.org/10.5194/acp-20-15147-2020, 2020.

Thorncroft, C. D. and Hodges, K.: African Easterly Wave Variability and Its Relationship to Atlantic Tropical Cyclone Activity, J. Clim., 14, 116–1179, https://doi.org/10.1175/1520-0442(2001)014%3C1166:AEWVAI%3E2.0.CO;2, 2001.

1 Thorncroft, C. D., Hall, N. M., and Kiladis, G. N.: Three-dimensional structure and
2 dynamics of African easterly waves, Part III: genesis., J. Atmos. Sci., 65, 3596–607,
3 https://doi.org/10.1175/2008JAS2575.1., 2008.

4 Weinzierl, B., Ansmann, A., Prospero, J., Althausen, D., Benker, N., and Chouza, F.: The
5 saharan aerosol long-range transport and aerosol–cloud-interaction experiment: Overview
6 and selected highlights, Bull. Amer. Meteor. Soc., 98, 1427–1451,
7 https://doi.org/10.1175/BAMS-D-15-00142.1, 2017.

8 Wilcox, E. M., Lau, W. K. M., and Kim, K. M.: A Northward shift of the North Atlantic
9 Ocean intertropical convergence zone in response to summertime Saharan dust outbreaks,
10 Geophys. Res. Lett., 37, L04804, https://doi.org/10.1029/2009GL041774., 2010.

11 Wright, J. S., Sun, X., Konopka, P., Krüger, K., Legras, B., Molod, A. M., Tegtmeier, S.,
12 Zhang, G. J., and Zhao, X.: Differences in tropical high clouds among reanalyses: origins
13 and radiative impacts, Atmos. Chem. Phys, 20, 8989–9030, https://doi.org/10.5194/acp-
14 20-8989-2020., 2020.

15 Wu, M. L. C., Reale, O., and Schubert, S. D.: A characterization of African easterly
16 waves on 2.5–6-day and 6–9-day time scales, J. Clim., 26, 6750–6774,
17 https://doi.org/10.1175/JCLI-D-12-00336.1, 2013.

18 Zhao, L., Lee, X., and Liu, S.: Correcting surface solar radiation of two data assimilation
19 systems against FLUXNET observations in North America, J. Geophys. Res. Atmos.,
20 118, 9552–9564, https://doi.org/10.1002/jgrd.50697., 2013.

21 Zuidema, P., Redemann, J., Haywood, J., Wood, R., Piketh, S., Hipondoka, M., and
22 Formenti, P.: Smoke and clouds above the southeast Atlantic: Upcoming field campaigns
23 probe absorbing aerosol's impact on climate, Bull. Amer. Meteor. Soc., 97, 1131–1135,
24 https://doi.org/10.1175/BAMS-D-15-00082.1, 2016.

1   **Table 1** MODIS and MERRA-2 data information applied in this study

Dataset	Product Name	Variables	Spatial Resolution	Temporal Resolution	Data Reference
MODIS	MOD08_D3	550-nm AOD, Deep-blue AOD	1°×1°	daily	Platnick (2015)
MERRA-2	M2I6NPANA	U, V, T, H	0.5°×0.625°	3-hourly (averaged to daily)	GMAO (2015a)
	M2T1NXRAD	$SWF_{TOA_{tot}}$, $SWF_{TOA_{clean}}$, $SWF_{sfc_{tot}}$, $SWF_{sfc_{clean}}$	0.5°×0.625°	1-hourly (averaged to daily)	GMAO (2015b)
	M2I3NPASM	Omega	0.5°×0.625°	3-hourly (averaged to daily)	GMAO (2015c)

3   **Table 2** The coordinates of domains of transient changes across the tropical Atlantic

4   Ocean:

AEW domains		
Description	Central Atlantic	Eastern Atlantic
Northern track waves	18° to 24°N -45° to -30°E	18° to 24°N -30° to -15°E
Downstream of jet-axis	12° to 18°N -45° to -30°E	12° to 18°N -30° to -15°E
Southern track waves	6° to 12°N -45° to -30°E	6° to 12°N -30° to -15°E

6
7
8
9
10

1   **Table 3** Summary of lag analyses showing AEWs evolution before and after dust peaks in

2   OSAL:

Downstream development of eddy activity – Central Atlantic			
	Before Dust-peak	Simultaneously at Dust-peak	After Dust-peak
Northern track AEWs	T < 0 Negligible changes in EKE	T = 0 EKE starts increasing	T = +3 Max EKE
Along the AEJ axis	T < 0 Negligible changes in EKE	T = 0 Decrease of EKE	T = +2 EKE starts increasing T ~ +3 to +4 Max EKE
Southern track AEWs	T = -3 EKE starts increasing	T = 0 Increase of EKE	T = +2 Max EKE
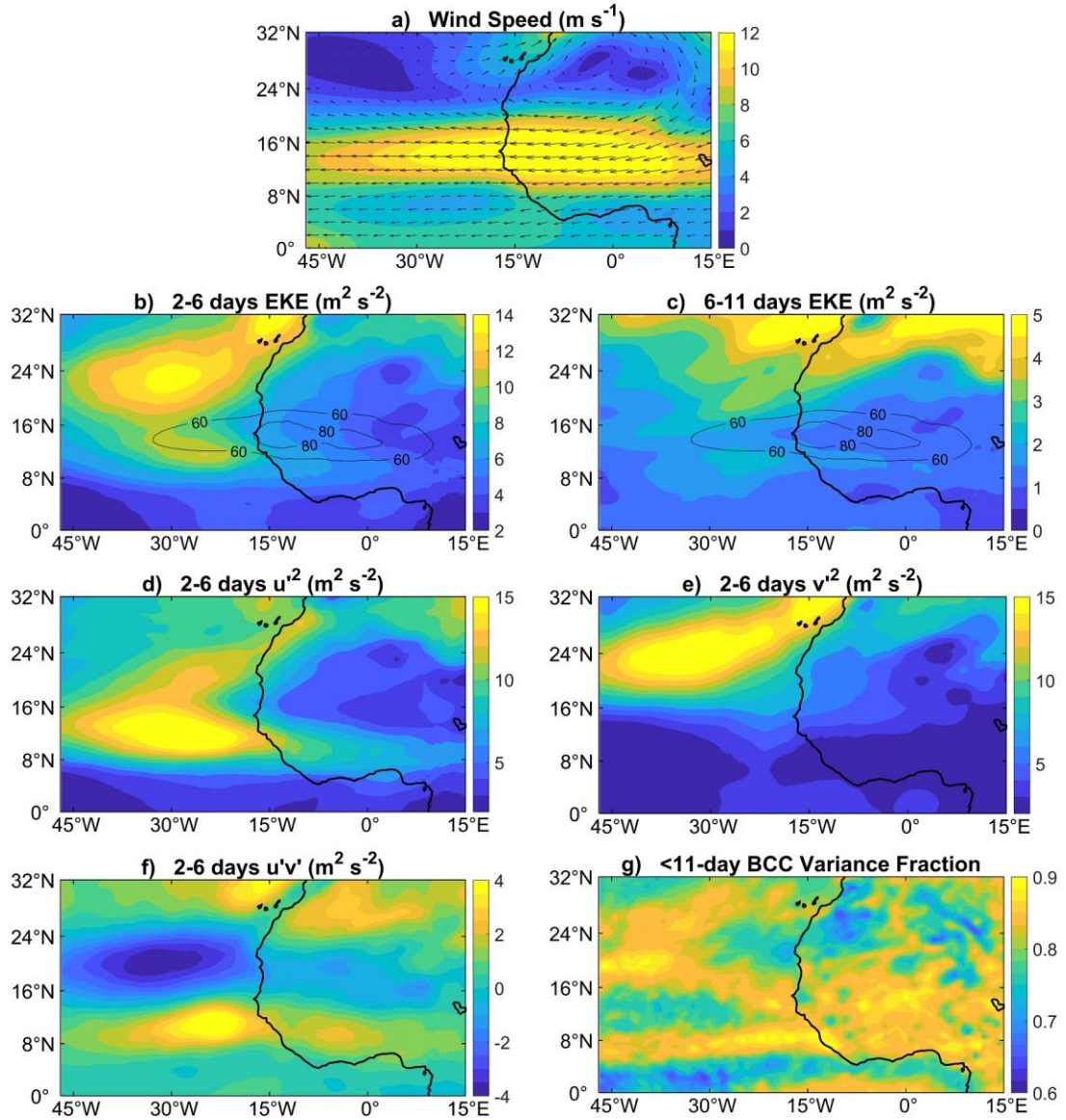
Figure 1 (a) Long-term mean of 600-hPa wind speed (ms^{-1}) from MERRA-2 reanalysis over JJA, 2000-2021. (b) Same as (a) but for 2-6-day bandpass filtered EKE (m^{2}s^{-2}) at 600-hPa. (c) Same as (b) but for 6-11-day bandpass filtered EKE. (d) Same as (b) but shows the 2-6-day variance of zonal wind, $\overline{u'^2}$, (m^{2}s^{-2}). (e) Same as (b) but shows the 2-6-day variance of meridional wind, $\overline{v'^2}$, (m^{2}s^{-2}). (f) Same as (b) but for the 2-6-day filtered transient momentum fluxes, $\overline{u'v'}$, (m^{2}s^{-2}). (g) Fraction of less than the 11-day variance of 600-hPa Baroclinic Conversion (BCC) with respect to the total variance of BCC in JJA, 2000-2021.
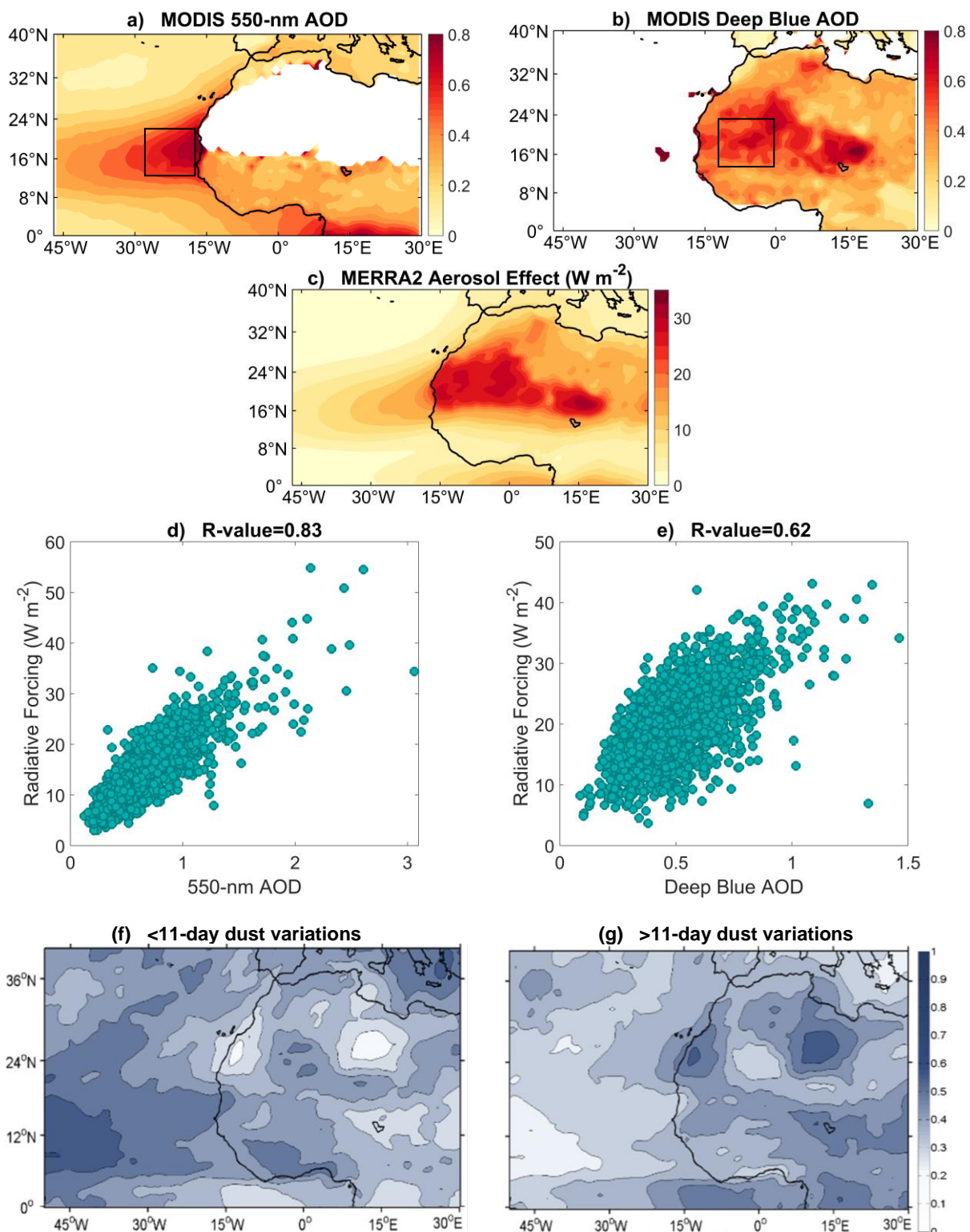
2 **Figure 2** (a) Long-term mean of 550-nm aerosol optical depth (AOD) from the MODIS over JJA, 2000-
3 2021. (b) Same as (a) but for 470-nm MODIS deep-blue AOD. (c) Same as (a) but for aerosol shortwave
4 radiative effect (Wm^{-2}) in the atmosphere (TOA minus surface) from the MERRA-2 reanalysis. (d)

1   Relationship between MODIS AOD and MERRA-2 radiative effect for JJA, 2000-2021. Each data point
2   shows daily data averaged over the OSAL region (rectangle in 2a). The results are statistically significant
3   with P-value < 0.05. (e) Same as (d), but for MODIS deep blue AOD over the land (rectangle in 1b). (f)
4   Fraction of variations of less than 11-day for the variance of aerosol radiative effect with respect to the total
5   variance using the long-term mean of aerosol radiative effect in the atmosphere (TOA minus surface) from
6   the MERRA-2 reanalysis over JJA, 2000-2021. (g) Same as (f) but for variations of more than 11-day.

Aerosol Radiative Effect (W m⁻²)
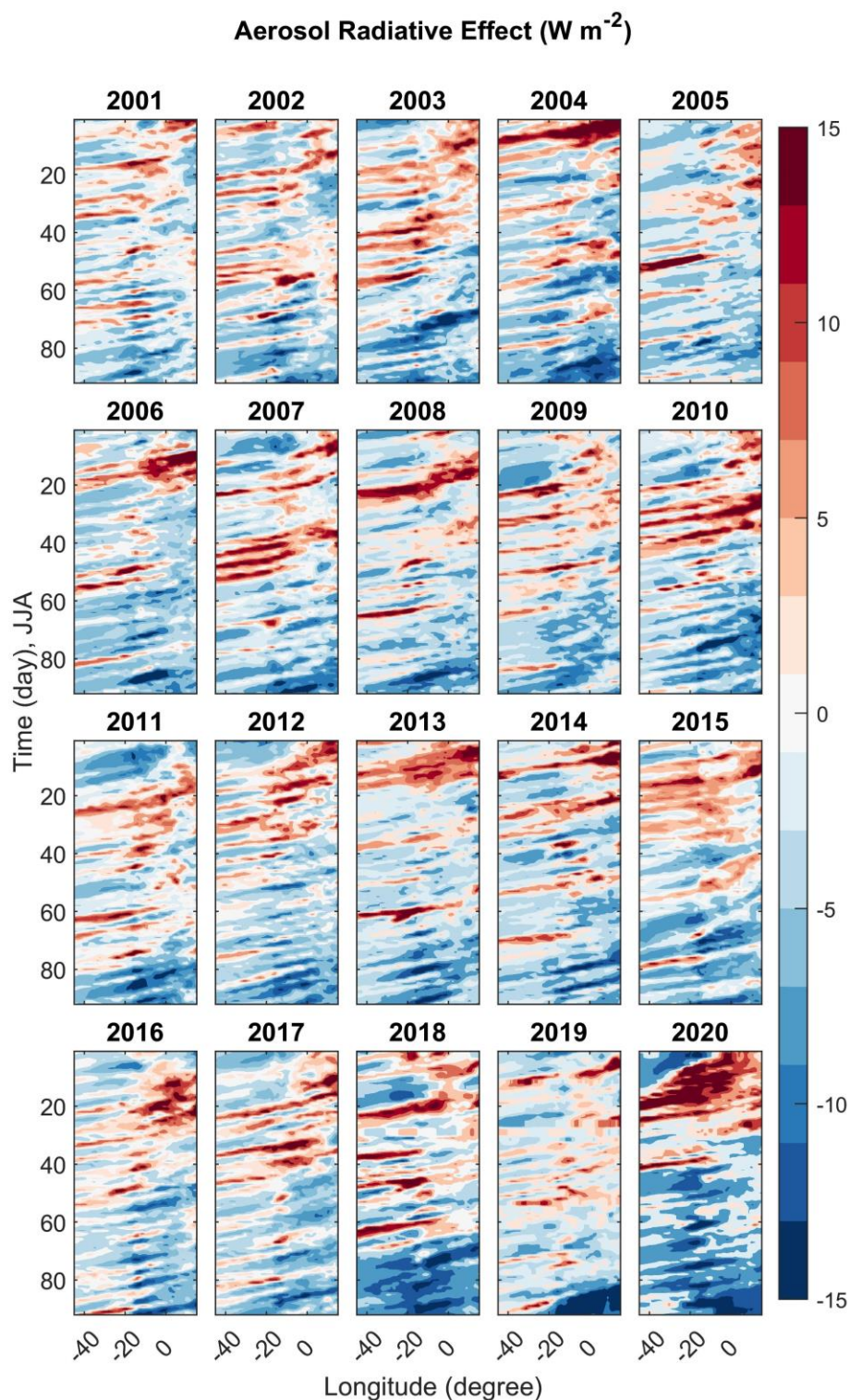
2 **Figure 3** Time-longitude Hovmöller diagrams of aerosol radiative effect daily anomalies (Wm⁻²) using the
3 MERRA-2 reanalysis for all individual boreal summer seasons, JJA from 2000 to 2021, meridionally
4 averaged (12-22° N) over the OSAL domain (rectangle in Figure 2a). Daily anomalies of aerosol radiative
5 effect are calculated with respect to the seasonal time average of radiative effect for each year.
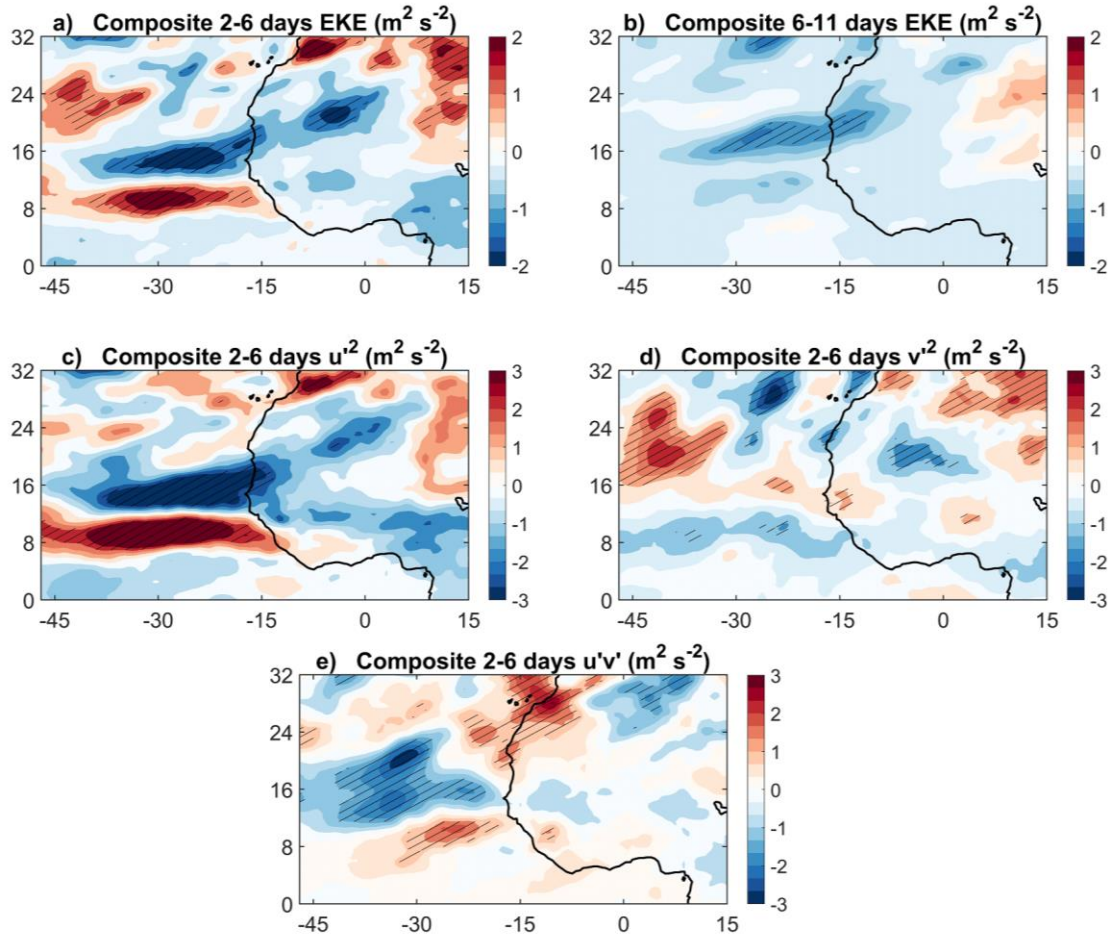
2 **Figure 4** (a) Composite 600-hPa 2-6-day filtered EKE (m^2s^{-2}) values for the times corresponding to the upper
3 quartile aerosol radiative effect minus the EKE values of the times corresponding to the lower quartile aerosol
4 radiative effect over the OSAL domain (rectangle in Figure 2a). The calculations are conducted using the
5 MERRA-2 reanalysis for JJA, 2000-2021. (b) Same as (a) but for 6-11-day filtered EKE (m^2s^{-2}). (c) same as
6 (a) but for the 2-6-day variance of zonal wind, $\overline{u'^2}$, (m^2s^{-2}). (d) As in (a) but for 2-6-day the variance of
7 meridional wind, $\overline{v'^2}$, (m^2s^{-2}). (e) Same as (a) but for the 2-6-day filtered momentum fluxes, $\overline{u'v'}$, (m^2s^{-2}).
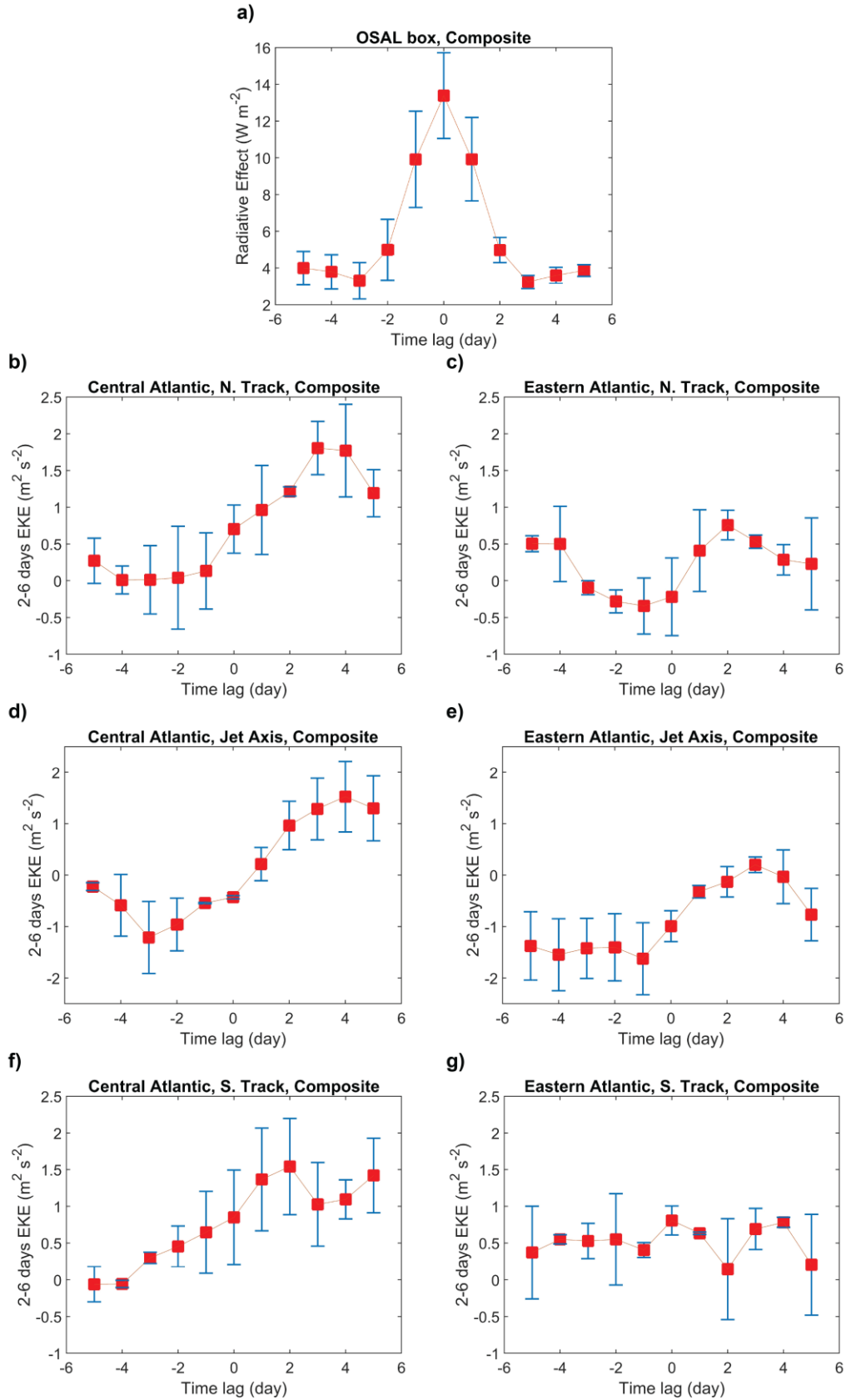
1 **Figure 5** (a) Daily time series of composite aerosol radiative effect for the days in the upper quartile minus
2 those days in the lower quartile radiative effect, spatially averaged over the OSAL domain (rectangle in
3 Figure 2a). T = 0 is assigned for the days with the highest variability of aerosol radiative effect in the
4 OSAL. T = +/- 1, T = +/- 2, T = +/- 3, T = +/- 4, and T= +/- 5 are assigned for five days before and five
5 days after each individual dust event, averaged over for 22 years, JJA, 2000-2021. (b) Same as (a) but for
6 the composite 2-6 day filtered EKE at 600-hPa, spatially averaged over the northern track AEWs in the
7 central Atlantic (18° to 24°N, -45° to -30°E). (c) Same as (b) but for the eastern Atlantic (18° to 24°N, -
8 30° to -15°E). (d) Same as (b) but spatially averaged over the domain, downstream of the AEJ in the central
9 Atlantic (12° to 18°N, -45° to -30°E). (e) same as (d) but for the eastern Atlantic (12° to 18°N, -30° to -
10 15°E). (f) same as (b) but spatially averaged over the southern track of the AEWs in the central Atlantic
11 (6° to 12°N, -45° to -30°E). (g) Same as (f) but for the eastern Atlantic (6° to 12°N, -30° to -15°E). The
12 domains of the wave activity are listed in Table 3.